Three-dimensional geometric analysis of the plunge centreless grinding process

N G Subramanya Udupa, MTech, **M S Shunmugam,** MSc(Eng), PhD and **V Radhakrishnan,** MTech, PhD
Department of Mechanical Engineering, Indian Institute of Technology, Madras, India

The grinding action and the rounding mechanism are highly complex in centreless grinding. The axis of the workpiece not only moves laterally but also tilts during the grinding process. Rowe and Barash have developed a two-dimensional model for an infeed centreless grinding neglecting the tilt of the workpiece.

In this paper, an attempt has been made to develop a simulation model which incorporates the tilt of the workpiece. The theoretical and experimental investigations have been carried out with workpieces having specific geometries and the results are discussed.

NOTATION

A_k	amplitude of the kth harmonic
A_d	amplitude of the dominant harmonic
d_w	diameter of workpiece
e_j	deviation of jth point from the least-squares circle
h	workpiece setting height
h_a	mean line average height
h_t	roundness error
k	order of the harmonic
k_{max}	order of the harmonic of maximum amplitude
K_m	machining elasticity parameter
L	length of workpiece
n	number of equispaced points on the roundness profile
N_a	average undulation number
$r(\theta)$	reduction in radius from the workpiece reference circle at an angle θ
$r(\theta - \alpha)$	magnitude of the error on the workpiece at the point where contact is made with the workplate
$r(\theta - \pi + \beta)$	magnitude of the error on the workpiece at the point where contact is made with the control wheel
R_0	radius of the least-squares circle
X_0, Y_0	coordinates of the centre of least-squares circle
α'	workplate angle
β	included tangent angle

1 INTRODUCTION

Centreless grinding is a unique and efficient process which is extensively used in the production of a wide variety of workpieces of circular cross-section. As the name of the process implies, the workpiece is not held between the centres but is supported by the workplate and the control wheel. The centre of the workpiece is kept above the line joining the centres of grinding and control wheels (Fig. 1a). The control wheel, which is a frictional driving element, governs the rotation of the workpiece. The process is highly complex and its rounding ability is affected by the geometric and dynamic stability of the workpiece. Hence, the quality of the ground parts, namely the out-of-roundness and surface finish, depends largely on the stability of the process. Attempts have been made to study the influence of the process parameters such as workpiece setting height, workplate angle, work speed, feedrate etc. on the quality of the ground components (**1–7**). Investigations have also been carried out to study the effect of high-material removal rate in centreless grinding, taking into account the variables such as the ratio of grinding wheel speed to work speed, work material etc. (**8–10**).

Controlling of roundness generally poses the greatest challenge. This is partly due to complexity in the mechanism of roundness generation in the centreless grinding process. The workpiece is supported on the surface that is being ground and, due to this, a feedback mechanism is automatically set up which often affects the quality of the ground parts.

A few attempts have been made to analyse the centreless grinding process with the aid of the geometric feedback mechanism. Rowe and Barash proposed a mathematical model to study the influence of parameters like included tangent angle, workplate angle, number of work revolutions etc. on the roundness error (**11**). An attempt to evaluate the roundness error and to analyse the harmonics of the waveform of the generated surface has also been made (**12**). Computer simulation techniques have been developed for the mechanism of centreless grinding to investigate the qualitative and quantitative effects of the process variables (**13**, **14**).

The mathematical procedures mentioned above do not take into account the tilt of the workpiece axis and therefore they are only two-dimensional models. Investigations have shown that the magnitude of the roundness error can vary from one end to the other of a single ground component (**13**). Drawn bars are, in many cases, used directly to form and finish parts on centreless grinders. In such cases the initial roundness error may vary from section to section along the length of the job. An irregularity at any section of the component may cause it to assume a tilted position, which in turn influences the rounding action throughout the length of the component. This may result in the generation of differ-

The MS was received on 22 October 1986 and was accepted for publication on 26 January 1987.

0263-7154/87 $2.00 + .05

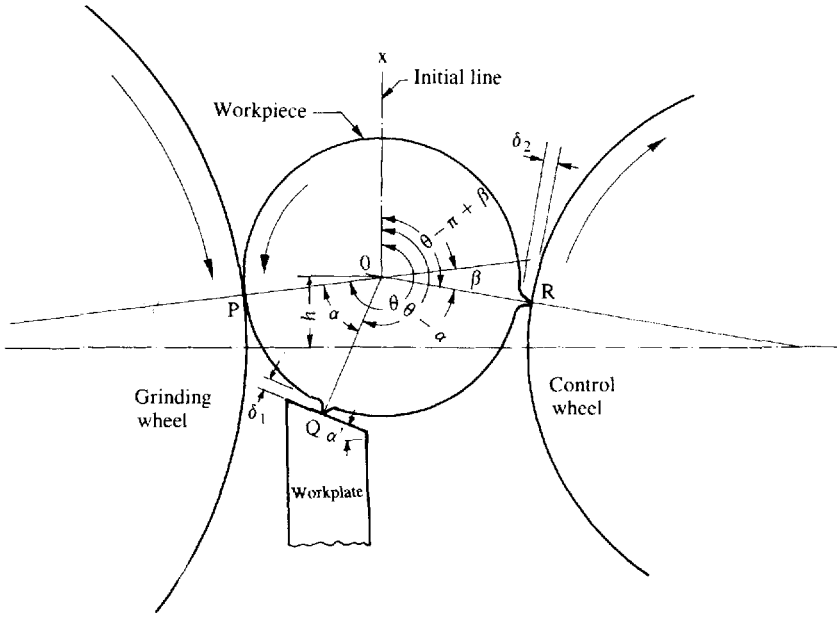

(a) Lateral movement in the transverse plane

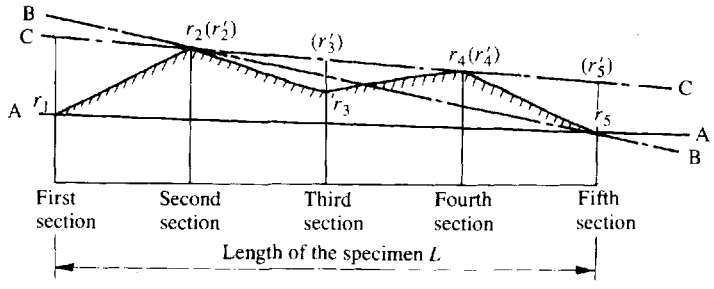

(b) Tilt in the longitudinal direction

Fig. 1 Determination of the workpiece movement in centreless grinding

ent circumferential profiles along the component's length. Hence, there is a need to simulate the centreless grinding, incorporating the effect of tilt, as a three-dimensional model.

This paper deals with a three-dimensional model developed to simulate the centreless grinding process. The roundness error predicted from the three-dimensional model is compared not only with those obtained from a two-dimensional model but also with the experimental results. Further, harmonic analysis of the theoretical and experimental roundness profiles is carried out to bring out the effectiveness of the three-dimensional simulation of the centreless grinding process. The results of theoretical and experimental investigations carried out in this connection are included in the paper.

2 SIMULATION OF CENTRELESS GRINDING PROCESS

2.1 Two-dimensional model

The two-dimensional approach attempted by several investigators is based on the equation of constraint (**11**, **14**). This equation quantifies the instantaneous change in the depth of cut due to workpiece displacements, which in turn occur due to radial deviations on the profile of the workpiece at the workplate and the control wheel.

The simulation of the centreless grinding process used here is based on a two-dimensional model proposed by Rowe and Barash (**11**). The geometrical details of the model for the case of infeed are shown in Fig. 1a. The true reduction in radius $r(\theta)$ of the workpiece in terms of the infeed $X(\theta)$ is given by

$$r(\theta) = K_m\left[X(\theta) - \left\{\frac{\sin\alpha}{\sin(\alpha+\beta)}\right\}r(\theta-\pi+\beta) + \left\{\frac{\sin\beta}{\sin(\alpha+\beta)}\right\}r(\theta-\alpha) - r(\theta-2\pi)\right] + r(\theta-2\pi) \quad (1)$$

where

$$\beta = \text{included tangent angle} = \sin^{-1}\left(\frac{2h}{d_g+d_w}\right) + \sin^{-1}\left(\frac{2h}{d_c+d_w}\right) \quad (2)$$

$$\alpha = \frac{\pi}{2} - (\alpha' + v\beta) \quad (3)$$

α' = workplate angle

$$v = \frac{1}{1 + (d_g + d_w)/(d_c + d_w)} \quad (4)$$

d_g = diameter of grinding wheel

d_c = diameter of control wheel

d_w = diameter of workpiece

h = workpiece setting height

K_m = machining elasticity parameter

In the simulation, the workpiece was divided into 360 equispaced radii. The magnitude of these radii at any given instant defined the shape of the workpiece. Next, the workpiece was rotated in steps of one degree. For each incremental movement, the values of $r(\theta - \alpha)$ and $r(\theta - \pi + \beta)$ which represented δ_1 and δ_2 were modified to account for the interference at the workplate and the control wheel respectively. The apparent depth of cut, given by the terms within parentheses of equation (1) could be negative in some circumstances. This amounted to replacing metal onto workpiece. In such a situation, no grinding could take place and $r(\theta)$ was replaced by $r(\theta - 2\pi)$. The workpiece material interfering with the grinding wheel surface was also identified and removed. An additional term incorporating the workpiece vibration with a specified amplitude can be added to equation (1). In the present investigation, this has not been incorporated as the main aim of the work is to study the geometric simulation of the process. The 360 values of $r(\theta)$ computed at the end of the first revolution were the input to the second revolution and provided the geometric feedback for the second revolution. 360 values of $r(\theta)$ computed at the end of a specified number of work revolutions defined the shape of the predicted roundness profile of the centreless ground component.

2.2 Three-dimensional model

The two-dimensional model described in Section 2.1 has certain limitations. For example, the two-dimensional model considers only the profile in the transverse section of the workpiece and an assumption is made that there is no variation in the longitudinal direction. However, a change in the longitudinal profile may have considerable influence on the generated profiles along the length of the workpiece. This limitation of the two-dimensional model can be overcome by going in for a three-dimensional model.

In this connection, it is to be mentioned that the irregularities on the workpiece profile before grinding may vary from a few micrometres to nearly a hundred micrometres. Measurements carried out on drawn bars, which are used directly in centreless grinding, showed humplike variations of height varying from a few to 80 micrometres. In addition, the initial shape of the profile was different from section to section with humps being distributed in a random manner throughout the length. Hence, the presence of such irregularities at different sections of the workpiece causes its axis to tilt during grinding. The effect of such tilting can be incorporated in the simulation only by going in for a three-dimensional model.

The simulation of the centreless grinding process using the three-dimensional model for the case of infeed is shown in the flow diagram (Fig. 2).

The initial shape of the cylindrical workpiece is defined by dividing the axis into a certain number of equispaced sections and dividing the profile at each section into 360 equispaced radii. For an incremental rotation of the workpiece, the values $r_i(\theta - \alpha)$ and

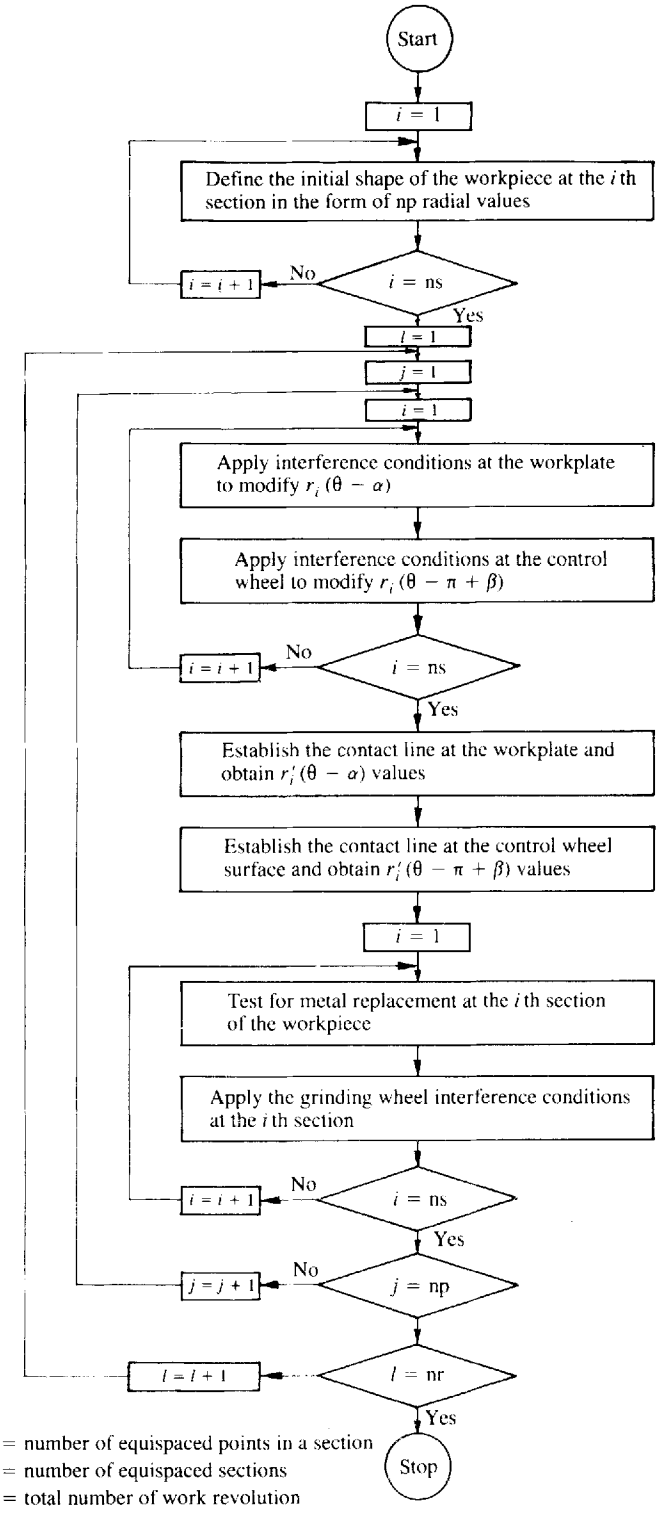

np = number of equispaced points in a section
ns = number of equispaced sections
nr = total number of work revolution
i = section under consideration
j = point considered in a section
l = work revolution

Fig. 2 Flowchart for the simulation of centreless grinding process: three-dimensional model

$r_i(\theta - \pi + \beta)$ at the ith section are modified as explained in Section 2.1, to take into account the interference at the workplate and the control wheel respectively. From one end to the other end of the workpiece, $r_i(\theta - \alpha)$ values are computed. These values decide the instantaneous line of contact of the workpiece with the workplate. Similarly, $r_i(\theta - \pi + \beta)$ values decide the instantaneous contact line of the workpiece with the control wheel. The contact lines determine the tilted position of the workpiece.

The contact lines are established so as to fulfil the following conditions:

1. The contact line has to pass through two points.
2. Being a crest line, it should not intersect the profile, that is all the deviations are either zero or negative with respect to the contact line.
3. The points of contact are well separated, as this condition corresponds to a stable position of the workpiece.

For example, let us consider the case shown in Fig. 1b. To establish the contact line, a trial line AA is passed through the end points r_1 and r_5. This line intersects r_2 and r_4 and condition 2 is contradicted. Now r_2 has maximum positive deviation. So r_1 is replaced by r_2 which is on the same side so as to satisfy the condition 3 mentioned above and a new line BB passing through r_2 and r_5 is established. With reference to this line, only r_4 has positive deviation. Hence, r_5 is replaced by r_4 and the next line CC is passed through r_2 and r_4. In the above case, since deviations at all the five sections are zero or less than zero, CC represents the instantaneous tilted position of the axis. Otherwise, this procedure is repeated until all the deviations are either negative or zero. If the maximum positive deviation occurs at the midpoint, then the minimum tilt condition is used to select the contact line.

After establishing the instantaneous tilted position of the axis of the workpiece, the radial values at the ith section are modified to $r'_i(\theta - \alpha)$ and $r'_i(\theta - \pi + \beta)$ so that they all lie on the respective contact lines. Also, the metal replacement condition and the grinding wheel interference restrictions are applied as in the case of the two-dimensional model.

The true reduction in radius $r_i(\theta)$ of the workpiece at the ith section is given by

$$r_i(\theta) = K_m\left[X(\theta) - \left\{\frac{\sin\alpha}{\sin(\alpha+\beta)}\right\} r'_i(\theta - \pi + \beta) + \left\{\frac{\sin\beta}{\sin(\alpha+\beta)}\right\} r'_i(\theta - \alpha) - r_i(\theta - 2\pi)\right] + r_i(\theta - 2\pi) \quad (5)$$

A FORTRAN program was developed to carry out the two- and three-dimensional simulations of the centreless grinding process, incorporating the interference restrictions, metal replacement and other conditions.

3 ROUNDNESS PROFILE ANALYSIS

The out-of-roundness and the mean line average height of the roundness profile are computed with reference to the least-squares circle. For this purpose, the radial deviations of the roundness profile are calculated using the linearized relation (**15**)

$$e(\theta_j) = r(\theta_j) - (R_0 + X_0 \cos\theta_j + Y_0 \sin\theta_j) \quad (6)$$

where

$$X_0 = 2\frac{\sum r(\theta_j)\cos\theta_j}{n}$$

$$Y_0 = 2\frac{\sum r(\theta_j)\sin\theta_j}{n}$$

$$R_0 = \frac{\sum r(\theta_j)}{n}$$

are the least-squares estimates and the summation is carried out from 1 to n where n is the number of equispaced points on the profile.

The roundness error in terms of the linearized values, $e(\theta_j)$, is given by

$$h_t = |e(\theta_j)_{max}| + |e(\theta_j)_{min}| \quad (7)$$

The mean line average height of the roundness profile is

$$h_a = \frac{\sum_{i=1}^{n} |e(\theta_j)|}{n} \quad (8)$$

The roundness profile is periodic in nature and repeats itself in each revolution. In such cases, the radial deviation $e(\theta_j)$ can be represented as a Fourier series given by

$$e(\theta_j) = \sum_{k=1}^{\infty} a_k \cos k\theta_j + \sum_{k=1}^{\infty} b_k \sin k\theta_j = \sum_{k=1}^{\infty} A_k \cos(k\theta_j - \psi_k) \quad (9)$$

where k represents the order of the harmonic. The Fourier coefficients a_k and b_k are given by

$$a_k = 2\frac{\sum e(\theta_j)\cos k\theta_j}{n}$$

$$b_k = 2\frac{\sum e(\theta_j)\sin k\theta_j}{n}$$

$$A_k = (a_k^2 + b_k^2)^{1/2}$$

$$\tan\psi_k = \frac{b_k}{a_k} \quad (10)$$

A_k and $\tan\psi_k$ represent the amplitude and phase of the kth harmonic respectively.

Spragg and Whitehouse suggested a parameter called the average undulation number which provides additional information about the roundness profiles (**16**). This parameter provides a quantitative basis for specifying the openness and closeness of the roundness profile. Hence, the average undulation number is also used to compare the theoretical roundness profiles of the three-dimensional model with that of the two-dimensional model and experimental roundness profiles.

The average undulation number is given by

$$N_a = \left\{ \frac{\sum_{k=1}^{m} k^2(a_k^2 + b_k^2)}{\sum_{k=1}^{m} (a_k^2 + b_k^2)} \right\}^{1/2} \quad (11)$$

where m represents the maximum harmonic number and is taken as 48.

4 RESULTS OF SIMULATION

Simulation procedures for two- and three-dimensional models explained in Section 2 hold good for any irregular initial shape of the workpiece. To bring out clearly the influence of tilting of the workpiece axis on the roundness error, simulation has been carried out on the workpieces having specific geometries as explained below.

Two- and three-dimensional simulation of the infeed grinding was carried out on a specimen with humps. The specimen selected as the humplike variation is a frequently encountered irregularity on drawn bars that in many cases go directly to centreless grinders.

The details of cylindrical workpieces with local hump/humps used in the simulation of the three-dimensional model and the equivalent workpieces with longitudinal hump/humps used in the two-dimensional model are given below:

1. Workpiece with one local hump at the front end and the equivalent workpiece with one longitudinal hump (Fig. 3a).
2. Workpiece with three local humps, one situated at the front end, the second at the middle section and the third at the rear end. The humps are at 120° to each other and the equivalent two-dimensional workpiece with three longitudinal humps at 120° are shown in Fig. 3b.

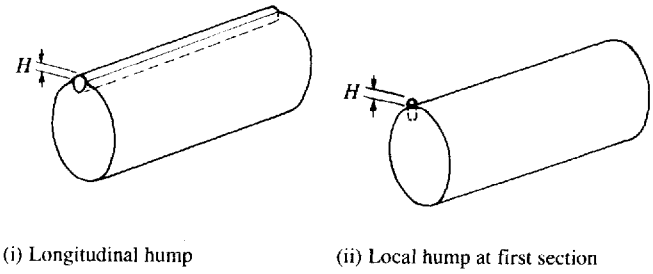

(i) Longitudinal hump (ii) Local hump at first section

(a) Workpiece with one hump

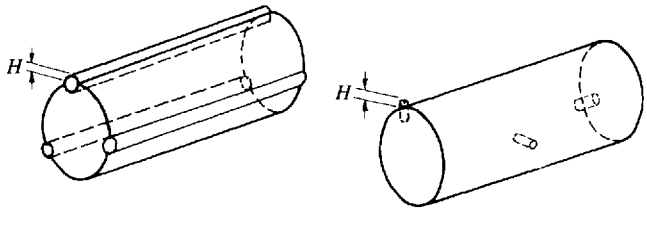

(i) Longitudinal humps at 120° (ii) Local humps, one each at first, third and fifth sections

(b) Workpiece with three humps

Fig. 3 Geometry of the workpieces used in simulation studies: $d_w = 30$ mm, $H = 40$ μm, $L = 60$ mm

A continuous uniform infeed of 1 μm per revolution of the workpiece was used in the simulation. The workpiece was allowed to complete 60 revolutions under uniform infeed conditions and then the conditions were held constant for 20 sparking-out revolutions.

Figure 4a shows the variation of the roundness error for the case of the workpiece with one hump as the grinding progresses for two- and three-dimensional models. In the case of the two-dimensional model, the roundness error reduces from 40 μm to about 3.85 μm in 80 work revolutions. The hump on the specimen causes the workpiece to move away from the grinding wheel surface when it comes in contact with the workplate. Similarly, any irregularity that comes in contact with the control wheel causes the workpiece to move towards the grinding wheel surface (Fig. 1a). These movements in the transverse plane result in the variation of the instantaneous depth of cut and affect the generated profile.

In the case of the three-dimensional model, the roundness error gradually decreases from 40 to 1.81 μm at the first section, that is at the section where the local hump is situated. At all other sections, namely the second to the fifth, where the initial roundness error is zero, the roundness error builds up during the first 20 revolutions [Fig. 4a(i)]. This is due to instantaneous tilting of the axis of the specimen in the grinding zone due to irregularity in the first section. The rate of building up of the roundness error is lowest at the fifth section and highest at the second section as they are farthest and nearest to the first section respectively. At the second to the fifth sections, where the initial roundness error was zero, the roundness error builds up to a sufficiently high value. Hence, after about 20 work revolutions, the instantaneous line of contact of the workpiece with either the workplate or the control wheel is influenced by the irregular profiles at these sections also. Ultimately, at the end of sparking the generated surface becomes smoother and more circular than the one produced by the two-dimensional model. From Table 1 it is seen that the roundness error predicted by the three-dimensional model is about 47 per cent of that predicted by the two-dimensional model.

The harmonic spectra of the roundness profiles shown in Fig. 4a(ii) bring out clearly the difference between the two- and three-dimensional models. In both the cases, the twentieth harmonic is the most dominant. This is mainly due to the set-up variables. However the magnitude of the twentieth harmonic based on the three-dimensional model is about 48 per cent lower than that of the two-dimensional model (Table 1). From the harmonic spectra, it is seen that harmonics such as the third, fifth, eighteenth etc., which are prominent in the two-dimensional case, are also prominent in the spectrum of the three-dimensional model, but their amplitudes are lower in the three-dimensional case. This reveals that the profiles generated by the three-dimensional model are smoother than those of the two-dimensional case.

The effect of work revolutions on the roundness error for the case of the workpiece with three local humps is shown in Fig. 4b(i). In the case of the two-dimensional model, the roundness error gradually decreases from 40 to about 6.0 μm. In the case of the three-dimensional model the roundness error reduces gradually from 40 to

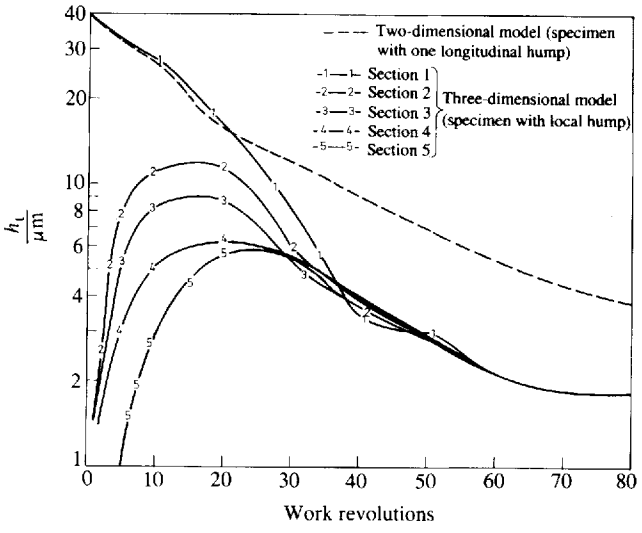

(i) Influence of work revolutions on the roundness error

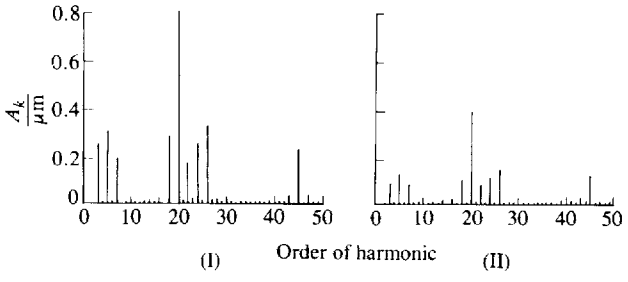

(ii) Harmonic spectra of theoretical roundness profiles: work revolutions = 80, d_w = 30 mm, L = 60 mm
(I) Two-dimensional model (longitudinal hump)
(II) Three-dimensional model (local hump at first section)

(a) Workpiece with one hump

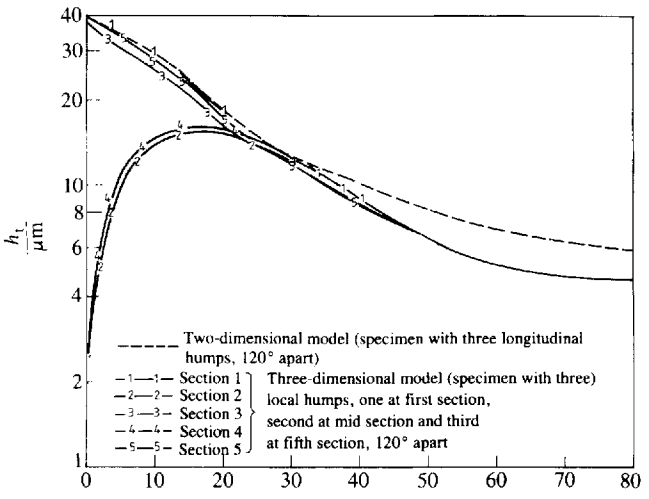

(i) Effect of work revolutions on the roundness error

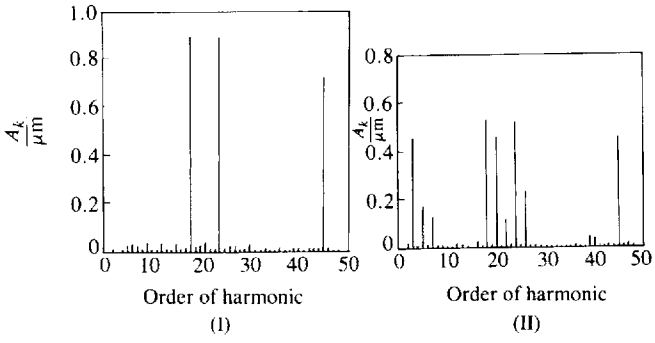

(ii) Harmonic spectra of theoretical roundness profiles
(I) Two-dimensional model (longitudinal humps)
(II) Three-dimensional models (local humps)

(b) Workpiece with three humps

Fig. 4 Comparison of two- and three-dimensional models

4.72 μm at the first, third and fifth sections, where the initial circularity error was 40 μm. At the second and fourth sections where the initial shape was perfectly circular, the out-of-roundness builds up in the initial stage and then gradually reduces. The roundness error predicted by the three-dimensional model is about 78 per cent of that obtained by the two-dimensional model (Table 2). From the harmonic spectra [Fig. 4b(ii)] of the simulated roundness profiles, it is seen that the eighteenth harmonic is the most dominant in both the two- and three-dimensional analyses.

From the above it is seen that, for the same set-up geometry, the workpiece with one hump resulted in 20 lobes and the workpiece with three humps produced 18 lobes. Also h_t and A_d in the case of one local hump were about 38 and 75 per cent of those corresponding to the workpiece with three local humps (Tables 1 and 2). Hence, as the number of humps increases, the amplitude of the dominant harmonic and the roundness error also increase.

Figure 5a to d shows the influence of the included tangent angle on the roundness error, mean line average height, amplitude of the dominant harmonic and the average undulation number for the case of the workpiece with one hump. It is seen that for $K_m = 0.08$, h_t reaches a minimum at $\beta = 8°$, whereas for $K_m = 0.3$, h_t reaches a minimum at $\beta = 6°$. In the case of the three-dimensional model, other parameters of the roundness

Table 1 Theoretical results for workpiece with one hump

Number of work revolutions = 80
Initial roundness error = 40 μm

Parameters	Two-dimensional model	Three-dimensional model				
		Sections				
		1	2	3	4	5
h_t(μm)	3.854	1.813	1.853	1.873	1.891	1.909
h_a(μm)	0.670	0.316	0.317	0.317	0.371	0.318
A_d(μm)	0.817	0.396	0.398	0.399	0.399	0.399
N_a	22.0	22.0	22.0	22.0	22.0	22.0

Table 2 Theoretical results for workpiece with three humps

Number of work revolutions = 80
Initial roundness error = 40 μm

Parameters	Two-dimensional model	Three-dimensional model				
		Sections				
		1	2	3	4	5
$h_t(\mu m)$	5.948	4.715	4.728	4.683	4.724	4.724
$h_a(\mu m)$	0.920	0.629	0.630	0.630	0.631	0.631
$A_d(\mu m)$	0.725	0.530	0.531	0.530	0.531	0.530
N_a	25.0	25.0	25.0	25.0	25.0	25.0

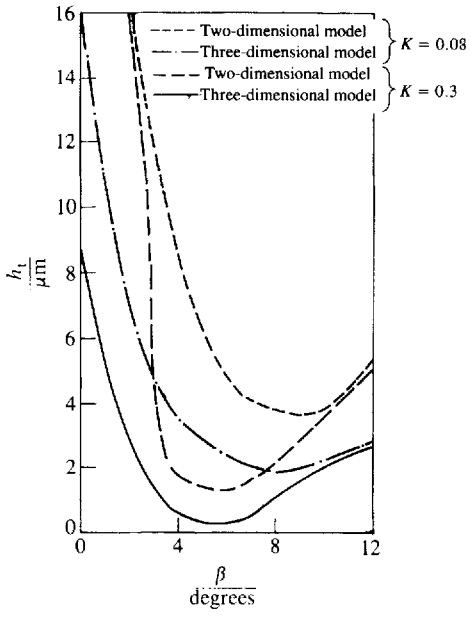

(a) Roundness error

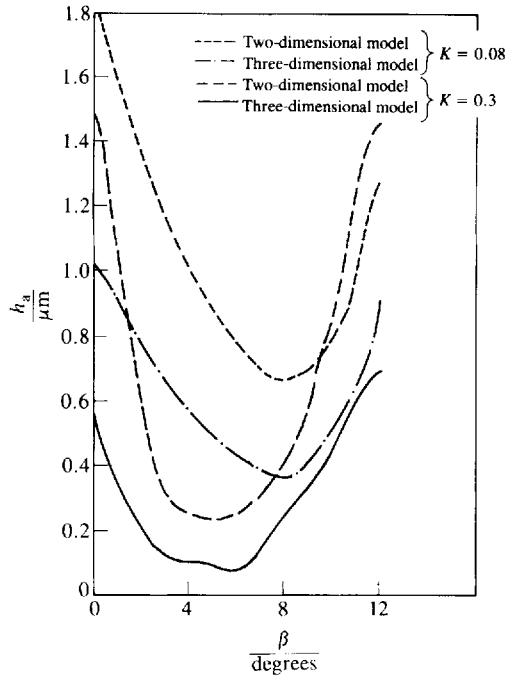

(b) Mean line average height

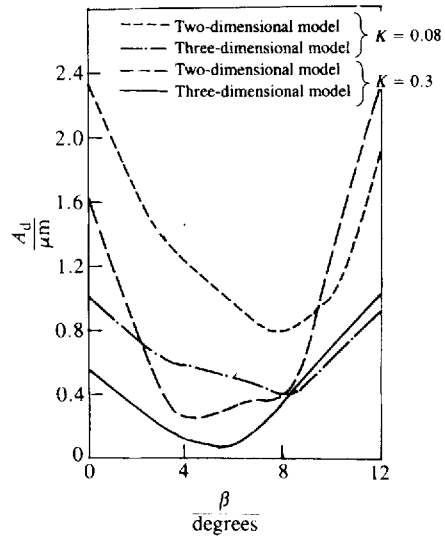

(c) Dominant harmonic amplitude

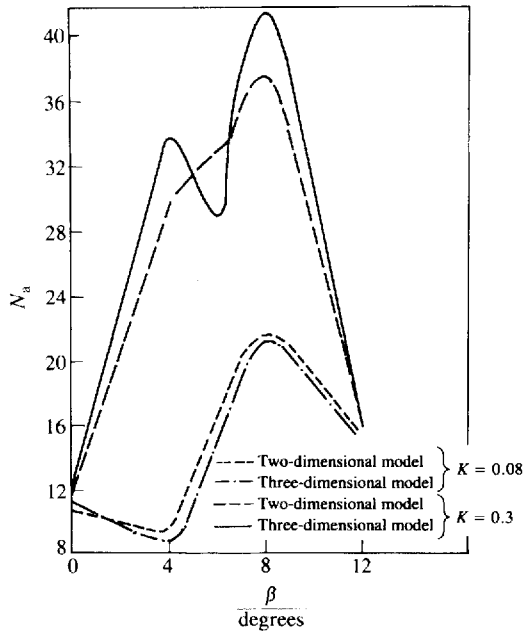

(d) Average undulation number

Fig. 5 Influence of the included tangent angle on the workpiece with one hump

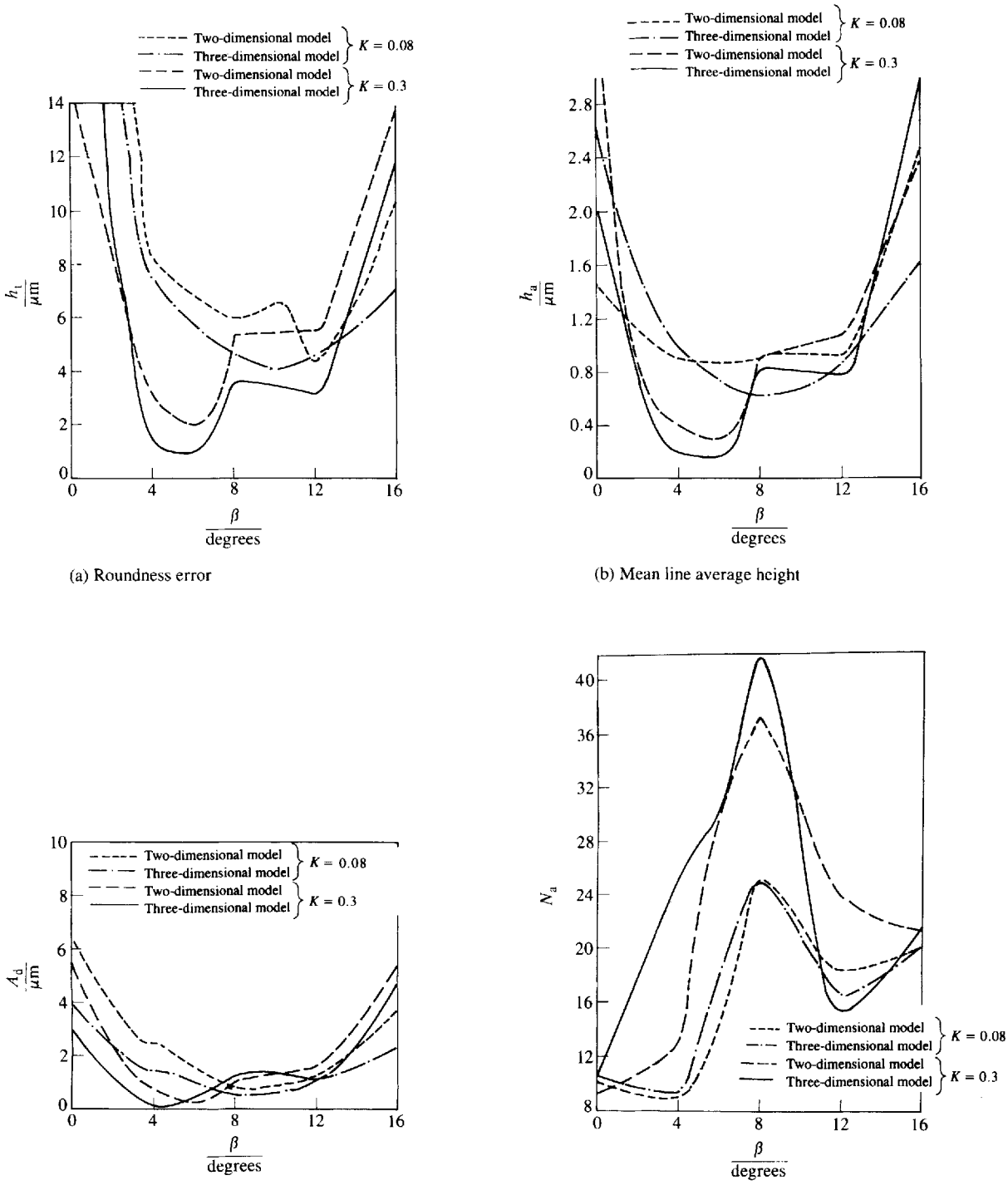

(a) Roundness error

(b) Mean line average height

(c) Dominant harmonic amplitude

(d) Average undulation number

Fig. 6 Effect of the included tangent angle on the workpiece with three humps

profile, namely h_a and A_d, reach a minimum at $\beta = 6$ and 8° for $K_m = 0.3$ and 0.08 respectively and N_a attains a maximum at $\beta = 8°$ for both the values of K_m (Fig. 5d).

It is also seen that in the case of the three-dimensional model and for $K_m = 0.3$ the values of h_t, h_a and A_d are less than those obtained for $K_m = 0.08$ and at all the values of β. Also at any given value of β, higher values of K_m increase N_a. From this it is clear that a machine with higher stiffness not only produces a smoother and more circular component but also permits the work to be ground better at a lower setting height.

Simulation of the process was also carried out on workpieces with multiple humps under varying conditions of the machine stiffness. The results showed trends similar to those corresponding to the workpiece with one hump. As all the results cannot be presented here, only a set of typical results pertaining to the case of the workpiece with three humps are given in Fig. 6a to d.

5 EXPERIMENTAL INVESTIGATION

5.1 Specimen preparation

The specimen with local and longitudinal humps was prepared as explained below. To prepare the local hump, as a first step, a blind radial hole was drilled at the front end of the cylindrical specimen. A cylindrical pin was press-fitted into this hole, such that the pin projected slightly above the surface of the cylinder. Next, the specimen was hand-finished carefully to get the desired shape and height for the hump (Fig. 3a).

In the case of the longitudinal hump, a through-hole was drilled in the specimen in the axial direction such that a cylindrical pin fitted into this hole projected slightly above the surface of the specimen and formed a longitudinal hump. Next, the projecting portion of the pin was hand-finished to achieve the desired geometric features. A few specimens with local and longitudinal humps were prepared as described above and the initial roundness profiles of the specimens were recorded on a roundness tester. A pair of specimens, one with local hump and the other with longitudinal hump, with closely matching hump shapes was selected for grinding in the experimental investigation. The harmonic amplitudes of the initial shape of the workpiece with hump is shown in Fig. 7a. Specimens with three local and longitudinal humps were also prepared in a similar way as that of one hump. The humps were formed at 120° to one another. In the case of the specimen with three local humps, humps were located at first, third and fifth sections (Fig. 3b). The harmonic amplitudes of the initial shape of the specimen with three humps is shown in Fig. 7b.

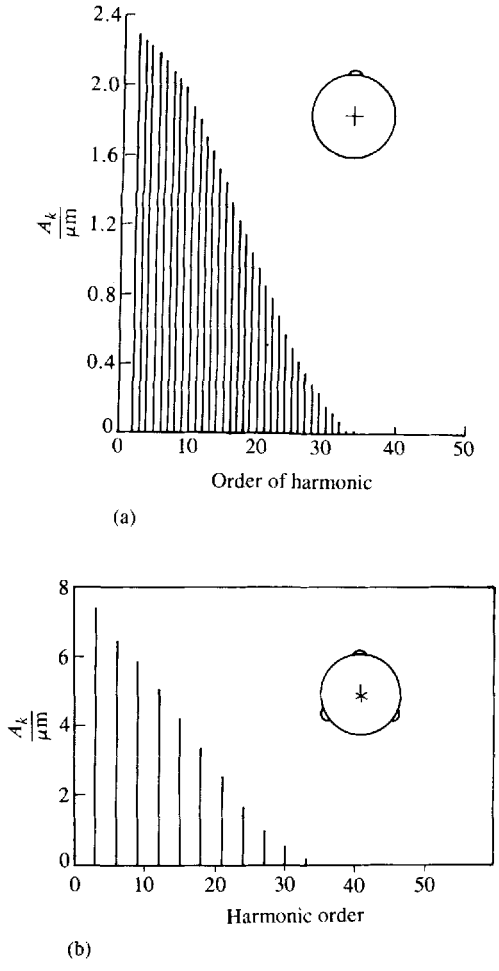

Fig. 7 (a) Harmonic amplitude spectrum of the initial shape of the workpiece with one hump
(b) Harmonic amplitude spectrum of the initial shape of the workpiece with three humps

5.2 Experimental results

Experiments were conducted on a 'Herminghausen' centreless grinding machine. Some relevant experimental details are given in the Appendix. The specimens were ground under uniform infeed conditions with a feedrate of 1 μm per revolution of the workpiece. The roundness profiles at different sections of the specimen were measured before and after grinding, on a Perthen roundness tester.

The results of the experimental investigation for the cases of specimens with one local and longitudinal humps are shown in Table 3 and a few typical roundness profiles of the ground parts are shown in Fig. 8a.

The ground specimen with local hump shows lower roundness error at all the five sections than that of the specimen with longitudinal hump (Table 3). The harmonic spectra of the ground specimen shown in Fig. 8b clearly bring out the fact that the generated profiles are more even in the case of the specimen with local hump. The mean line average height and the amplitude of the dominant harmonic in the case of the specimen with longitudinal hump are much higher than those of the specimen with local hump. For example, in the case of the specimen with local hump, the mean line average height and the dominant harmonic amplitude are about 30 and 27 per cent of the corresponding values of the

Table 3 Experimental results for specimen with one hump

Number of work revolutions = 80
Initial roundness error = 40 μm

	Specimen with one hump					
		Local				
		Sections				
Parameters	Longitudinal	1	2	3	4	5
h_t(μm)	9.645	5.449	5.520	5.631	4.721	4.001
h_a(μm)	1.784	0.534	0.502	0.512	0.468	0.398
A_d(μm)	1.380	0.372	0.350	0.322	0.290	0.244
N_a	21.0	26.0	25.0	25.0	26.0	28.0

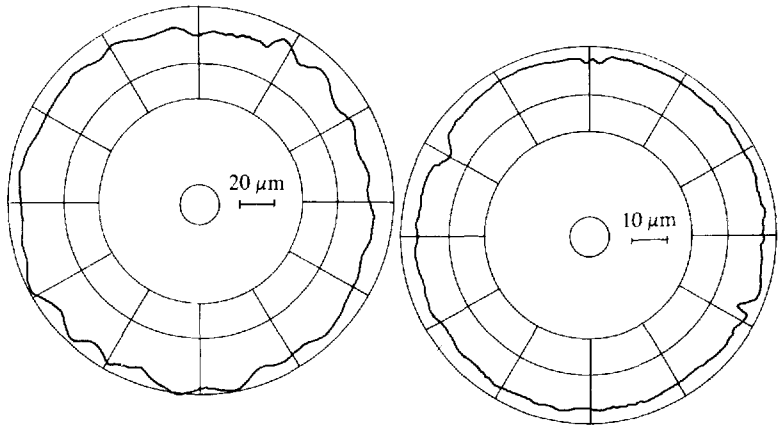

(i) Ground specimen with longitudinal hump

(ii) First section of ground specimen with local hump

(a) Typical polar charts

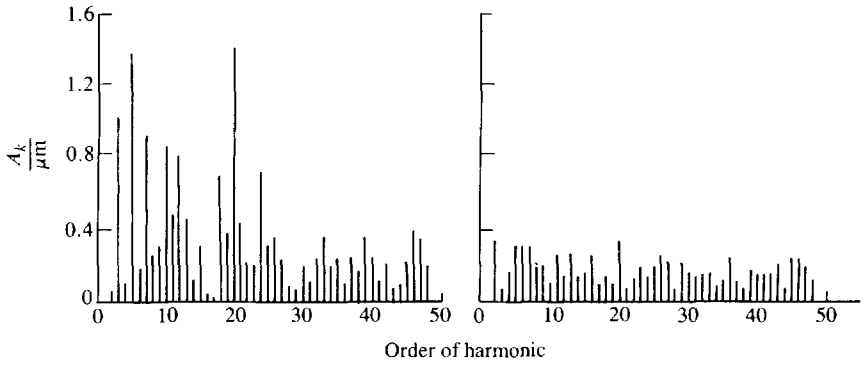

(i) Ground specimen with longitudinal hump

(ii) First section of ground specimen with local hump

(b) Harmonic spectra of the polar charts

Fig. 8 Experimental results: specimen with one hump (work revolutions = 80, d_w = 30 mm, L = 60 mm)

ground specimen with longitudinal hump (Table 3). The average undulation number is also higher in the case of the specimen with local hump, showing greater closeness of the roundness profile.

Some interesting similarities are also there between the theoretical and experimental results pertaining to the one-hump case. In both the cases, the twentieth harmonic is dominant. Further, the other harmonics which are prominent in the theoretical harmonic spectra are also prominent in the harmonic spectra of the experimental roundness profiles. Also the ratio of the roundness error based on the two-dimensional model to that of the three-dimensional model is approximately the same as the ratio of the roundness error of the ground specimen with the longitudinal hump to that of local hump. Another salient feature is that the harmonic spectra based on the three-dimensional model and that of the ground specimen with the local hump show that the surfaces generated in both the cases are smooth and even.

Figure 9a and b shows the roundness profiles of the ground parts and the harmonic spectra of the roundness profiles for the case of the specimen with three humps. The values of h_t, h_a, A_d and N_a measured at different sections of the ground specimen are presented in Table 4. The results show that the profiles of the

Table 4 Experimental results for specimen with three humps

Number of work revolutions = 80
Initial roundness error = 40 μm

	Specimen with three humps					
		Local				
		Sections				
Parameters	Longitudinal	1	2	3	4	5
$h_t(\mu m)$	15.22	7.28	7.196	6.632	7.024	7.865
$h_a(\mu m)$	3.040	0.463	0.410	0.590	0.430	0.640
$A_d(\mu m)$	4.910	0.340	0.380	0.634	0.470	0.580
N_a	10.0	27.0	28.0	24.0	25.0	23.0

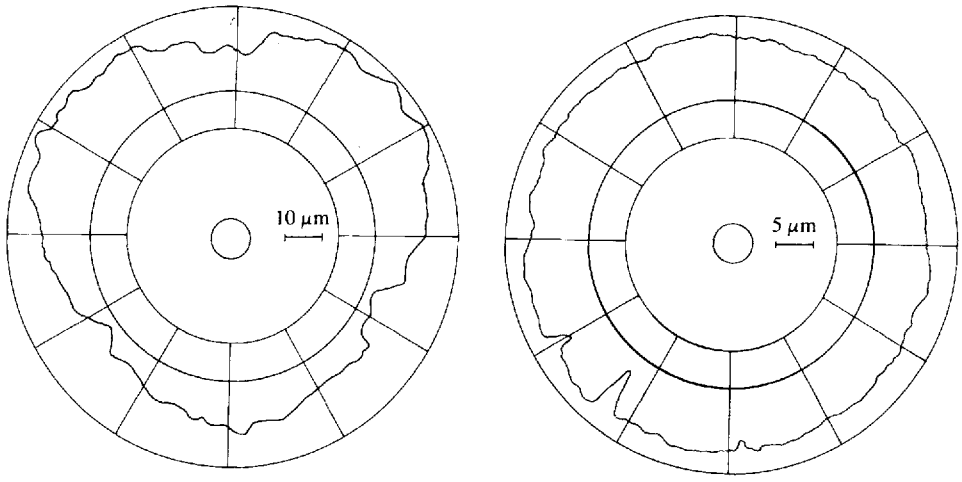

(i) Ground specimen with three longitudinal humps

(ii) First section of ground specimen with three local humps

(a) Typical polar charts

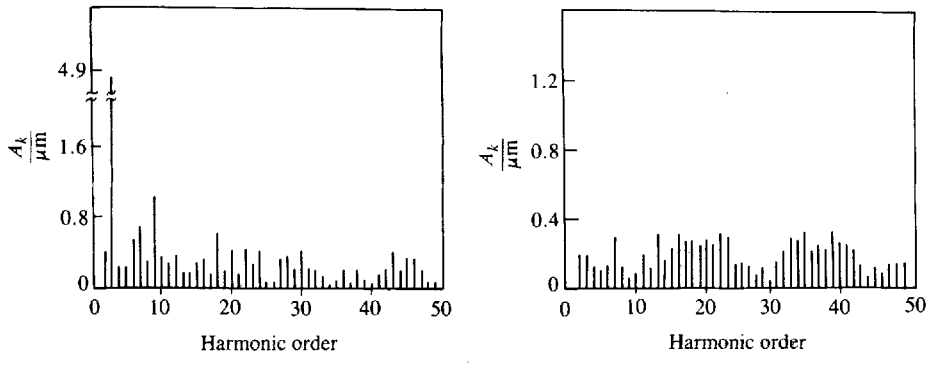

(i) Ground specimen with three longitudinal humps

(ii) First section of ground specimen with three local humps

(b) Harmonic spectra of the polar charts

Fig. 9 Experimental results: specimen with three humps

ground parts with local humps in this case also generate smoother and more even surfaces than those of the specimen with three longitudinal humps. From the above comparison of the experimental and theoretical results, it is clear that the axis of the specimen with local hump undergoes tilting during grinding, as described in the three-dimensional model. Hence, the simulation of the centreless grinding process taking into account the tilting of the axis is closer to a practical situation where the local irregularities at one section can influence the surface generated at other sections of the workpiece. On the other hand, the two-dimensional model is an approximate case and holds good for the cases where the initial shape of the specimen remains the same at all the sections. This is evident from the common features that the results of the two-dimensional model have with the experimental results of the longitudinal hump case. Another point to be observed is that for a given value of machining elasticity parameter, the three-dimensional model predicts a lower roundness error than the two-dimensional model.

6 CONCLUSIONS

The two-dimensional model is a limiting case and can take into account the movement of the workpiece in the transverse plane only. On the other hand, the three-dimensional model incorporates the tilt of the workpiece also.

The roundness error predicted by the three-dimensional model is much lower than that of the two-dimensional model. Also, the profiles generated are smoother and more even in the three-dimensional case.

Comparison of theoretical and experimental results has shown that the three-dimensional model is closer to practical situations.

In addition to set-up geometry, the initial shape of the workpiece also significantly influences the generated surface. As the number of humps increases, the amplitude of the dominant harmonic and the roundness error also increase. Therefore a grinding machine with greater stiffness not only produces a smoother and a more circular profile but also permits the workpiece to be

ground better at a lower setting height than that of a machine with lower stiffness.

In actual grinding practice, in addition to initial irregularities, the workpiece may vibrate under unstable conditions. By using a known pattern of workpiece vibration as input, the behaviour of the workpiece can be studied with better clarity with the aid of the three-dimensional model.

The proposed method of simulation goes much further in analysing the geometric stability of the process. This helps in better understanding of the complex generating mechanism of the centreless grinding and aids in closer control of the roundness error.

REFERENCES

1 **Rowe, W. B.** Research into mechanics of centreless grinding. *Precision Engng*, 1979, **1**, 75–84.

2 **Frost, M.** and **Fursdon, P. M. T.** Towards optimum centreless grinding. *Proc. of Milton C. Shaw Grinding Symp.*, 1985, **16**, 3213–3218 (ASME, New York).

3 **Subramanya Udupa, N. G., Shunmugam, M. S.** and **Radhakrishnan, V.** Influence of workpiece position on roundness error and surface finish in centreless grinding. *Int. J. Mach. Tools Manufact.*, 1987, **27**, 77–89.

4 **Miyashita, M., Hashimato, F.** and **Kanai, A.** Diagram for selecting chatter free conditions of centreless grinding. *Ann. CIRP*, 1982, **31**, 221–223.

5 **Drobashvskii, G. S.** Optimum settings for a centreless grinder. *Mach. Tooling*, 1973, **20**, 20–21.

6 **Subramanya Udupa, N. G., Shunmugam, M. S.** and **Radhakrishnan, V.** Process monitoring in centreless grinding for out-of-roundness and surface finish criteria. *Proc. 12th All India Mach. Tool Des. Res. Conf.*, 1986, 316–320.

7 **Subramanya Udupa, N. G., Shunmugam, M. S.** and **Radhakrishnan, V.** Preliminary investigations on the surface finish and roundness error in centreless grinding. *Proc. 11th All India Mach. Tool Des. Res. Conf.*, 1984, 251–258.

8 **Bell, W. F., Brough, D.** and **Rowe, W. B.** Achieving and monitoring high rate centreless grinding. *Proc. Int. Conf. Mach. Tool Des. Res.*, 1983, **24**, 313–322.

9 **Bell, W. F., Brough, D.** and **Rowe, W. B.** High rate centreless grinding of ferrous components. *Proc. Int. Conf. Mach. Tool Des. Res.*, 1984, **25**, 269–275.

10 **Rowe, W. B., Bell, W. F.** and **Brough, D.** Optimization studies in high removal rate in centreless grinding. *Ann. CIRP*, 1986, **35**, 235–238.

11 **Rowe, W. B.** and **Barash, M. M.** Computer method for investigating the inherent accuracy of centreless grinding. *Int. J. Mach. Tool Des. Res.*, 1964, **4**, 91–116.

12 **Chien, A. Y.** The rounding-off theory of centreless grinding. *Int. J. Mach. Tool Des. Res.*, 1981, **21**, 49–55.

13 **Bhateja, C. P.** Current state of the art of workpiece roundness control in precision centreless grinding. *Ann. CIRP*, 1984, **33**, 199–203.

14 **Rowe, W. B., Barash, M. M.** and **Koenigsberger, F.** Some roundness characteristics of centreless grinding. *Int. J. Mach. Tool Des. Res.*, 1965, **5**, 203–215.

15 **Shunmugam, M. S.** On assessment of geometric errors, *Int. J. Prod. Res.*, 1986, **24**, 413–425.

16 **Spragg, R. C.** and **Whitehouse, D. J.** A new unified approach to surface metrology. *Proc. Instn Mech. Engrs*, 1970–1, **185**, 697–707.

APPENDIX

Experimental conditions:

Grinding machine	Herminghausen SR-2G model
Grinding wheel	300 mm diameter, A60 MV
Grinding wheel speed	2000 r/min
Control wheel	200 mm diameter, rubber bonded
Control wheel speed	30 r/min
Workplate angle	30°
Included tangent angle	8°
Coolant	emulsion